Sampling and Reconstruction on a Diamond Grid and the Tetrahedral Digital Waveguide Mesh

Brian Hamilton, *Student Member, IEEE*

Abstract

It is shown that half of the points on the diamond grid are redundant for sampling and reconstructing a bandlimited 3-D signal. This redundancy is then exploited to show that the tetrahedral digital waveguide mesh requires four times more computational density and twice the memory storage for the same approximation as a finite difference scheme on the face-centered cubic lattice.

Index Terms

Multidimensional sampling, finite difference method, digital waveguide mesh, artificial reverberation.

I. Introduction

It has long been established that the body-centered cubic lattice (BCC) is the optimal lattice for 3-D sampling of bandlimited signals [1]. The face-centered cubic (FCC) lattice is nearly-optimal [1], [2] and is another viable alternative to the standard cubic lattice. The suitability of the diamond grid [3] for 3-D sampling has also been studied [4], [5].

These grids play another role in finite difference (FD) [6] and digital waveguide mesh (DWM) [7], [8] methods for artificial reverberation [9] and 3-D room acoustics simulations [4], [10]–[13]. In these numerical methods, the solution to the 3-D wave equation is approximated at points on a spatial grid, at discrete steps in time. A continuous spatial approximation to a 3-D acoustic field can then be reconstructed

Manuscript received April XX, 2013; revised July XX, 2013; accepted July XX, 2013; Date of publication July XX, 2013.

This work was supported by the European Research Council, under grant StG-2011-279068-NESS, and by the Natural Sciences and Engineering Research Council of Canada.

The author is with the Acoustics and Audio Group, University of Edinburgh, UK (e-mail: b.hamilton-2@sms.ed.ac.uk).

at each time-step. Aside from at the initial conditions, sampling is not part of the FD approximation (in most cases, the solution is unknown and therefore cannot be sampled), but the reconstruction and maximum bandwidth in the approximation follows from multidimensional sampling theory [1], [4], [14].

Numerical dispersion is the main concern in 3-D room acoustics applications of these methods, since it can lead to audible artifacts (smearing of transients). It has been reported that the tetrahedral DWM on the diamond grid has favourable numerical dispersion [4], [7], and it has been used for 3-D room acoustics modelling [11], [12], but its complex geometry makes it difficult to use in practice [13]. The computational efficiency of these methods, in terms of minimising numerical dispersion, is of great importance since simulations of large 3-D spaces at audio rates (e.g. 44.1 kHz) carry heavy computational costs and can be long even with the help of graphics processing units (GPUs) [15]. As such, the computational efficiency of DWM and FD schemes has been the subject of many studies [4], [8], [13], [14], [16]. The tetrahedral DWM and its equivalent FD scheme have been left out of recent studies comparing FD schemes [13], [16] due to its complicated structure, so its suitability for 3-D room acoustics simulations remains an open question [13].

The purpose of this letter is to answer this question on the tetrahedral DWM. First, sampling and reconstruction on the diamond grid will be addressed, then it will be shown that the tetrahedral DWM can be replaced by a 13-point FD scheme on the FCC lattice with substantial savings in memory and computation.

II. Sampling on the diamond grid

The FCC lattice, the diamond grid, and the BCC lattice can be described by a general construction [3]. Let $\boldsymbol{a}_1 = (0,0,0)$, $\boldsymbol{a}_2 = (\frac{1}{2},\frac{1}{2},\frac{1}{2})$, $\boldsymbol{a}_3 = (\frac{1}{2},\frac{1}{2},-\frac{1}{2})$, and $\boldsymbol{a}_4 = (1,0,0)$. Consider the grids, or sets of points, defined by:

$$\boldsymbol{P}_M = \bigcup_{m=1}^{M} \{\varepsilon(\boldsymbol{x} + \boldsymbol{a}_m) : \boldsymbol{x} \in \mathbb{Z}^3, (x_1 + x_2 + x_3) \bmod 2 = 0\}, \tag{1}$$

where $\varepsilon \in \mathbb{R}$ is an arbitrary scaling factor. These are displayed in Fig. 1. The FCC lattice, denoted by $\boldsymbol{F}$, is simply $\boldsymbol{F} = \boldsymbol{P}_1$. The diamond grid, denoted by $\boldsymbol{D}$, is two shifted FCC lattices: $\boldsymbol{D} = \boldsymbol{P}_2$. The BCC lattice, denoted by $\boldsymbol{B}$, is four shifted FCC lattices: $\boldsymbol{B} = \boldsymbol{P}_4$. The significance of $\boldsymbol{P}_3$ will be discussed shortly.[1] A lattice is a set of points (vectors) that forms an additive group [3] so $\boldsymbol{D}$ and $\boldsymbol{P}_3$ are not lattices. Let $\boldsymbol{F}_1 = \boldsymbol{F}$, and $\boldsymbol{F}_i = \{\boldsymbol{P}_i \setminus \boldsymbol{P}_{i-1}\}$ for $i \in \{2,3,4\}$ denote the individual shifted FCC sublattices.

[1]It is worth noting that $\boldsymbol{P}_3$ is the vertex arrangement of the space-filling tessellation that uses rhombic dodecahedral cells.

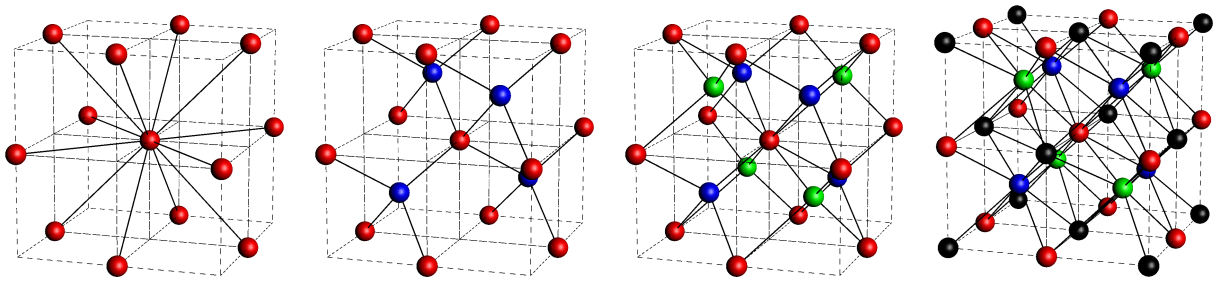

(a) $\boldsymbol{P}_1$ (b) $\boldsymbol{P}_2$ (c) $\boldsymbol{P}_3$ (d) $\boldsymbol{P}_4$

Fig. 1: Points of $\boldsymbol{P}_M$ within a cube with vertices $(\pm\varepsilon, \pm\varepsilon, \pm\varepsilon)$. Colours distinguish FCC sublattices. Solid lines connect nearest neighbouring points.

Let $f(\boldsymbol{x})$ be a 3-D signal, where $\boldsymbol{x} \in \mathbb{R}^3$, and let $s_{\boldsymbol{v}}$ denote the spatial shift operator: $s_{\boldsymbol{v}} f = f(\boldsymbol{x} - \boldsymbol{v})$, where $\boldsymbol{v} \in \mathbb{R}^3$. Define a "sampling lattice" for some grid of points $\boldsymbol{G}$ as:

$$\text{Ш}_{\boldsymbol{G}}(\boldsymbol{x}) = \sum_{\boldsymbol{v} \in \boldsymbol{G}} s_{\boldsymbol{v}} \delta(\boldsymbol{x}) \,, \quad \boldsymbol{x} \in \mathbb{R}^3 \,, \tag{2}$$

where $\delta(\boldsymbol{x})$ denotes a spatial Dirac delta. "Sampling" can be represented by the multiplication with $\text{Ш}_{\boldsymbol{G}}$, and a "sampled signal" is simply $f_{\boldsymbol{G}}(\boldsymbol{x}) = (\text{Ш}_{\boldsymbol{G}} f)(\boldsymbol{x})$ [1], [17]. The sampled signal $f_{\boldsymbol{G}}(\boldsymbol{x})$ can also said to be "discretised", but discretisation does not necessarily imply sampling was performed; this will be important when considering FD approximations. The spatial Fourier transform (FT) of $f(\boldsymbol{x})$ is defined as follows:

$$\widehat{f}(\boldsymbol{\xi}) = \int_{\boldsymbol{x} \in \mathbb{R}^3} f(\boldsymbol{x}) e^{-\jmath 2\pi \boldsymbol{x} \cdot \boldsymbol{\xi}} d\boldsymbol{x} \,, \quad \boldsymbol{\xi} \in \mathbb{R}^3 \,, \tag{3}$$

where $\boldsymbol{\xi}$ is the spatial frequency, $\jmath = \sqrt{-1}$, and let $\mathcal{F}(f) = \widehat{f}$. The FT of $\text{Ш}_{\boldsymbol{L}}(\boldsymbol{x})$, where $\boldsymbol{L}$ is some lattice, can be written as [2], [5], [17]:

$$\widehat{\text{Ш}}_{\boldsymbol{L}}(\boldsymbol{\xi}) = \frac{1}{|\det \mathbf{V}|} \sum_{\boldsymbol{v} \in \boldsymbol{L}^*} s_{\boldsymbol{v}} \delta(\boldsymbol{\xi}) \,, \quad \boldsymbol{\xi} \in \mathbb{R}^3 \,, \tag{4}$$

where $\mathbf{V}$ is a square matrix used to generate the lattice $\boldsymbol{L}$ with the construction: $\boldsymbol{L} = \{\mathbf{V}\boldsymbol{m} : \boldsymbol{m} \in \mathbb{Z}^3\}$ and where $\boldsymbol{L}^*$ is the dual lattice of $\boldsymbol{L}$, given by $\boldsymbol{L}^* = \{\mathbf{V}^{-T}\boldsymbol{m} : \boldsymbol{m} \in \mathbb{Z}^3\}$ [3]. For example, the lattice $\boldsymbol{F}$ can be generated using the matrix $\mathbf{V} = \varepsilon(\mathbf{1} - \mathbf{I})$ and one arrives at $\boldsymbol{F}^* = \boldsymbol{B}/\varepsilon^2 \Rightarrow \boldsymbol{B}^* = \boldsymbol{F}/\varepsilon^2$ [3]. The *support* of f is defined as $\operatorname{supp} f = \{\boldsymbol{x} \in \mathbb{R}^3 : f(\boldsymbol{x}) \neq 0\}$. Let $\boldsymbol{G}^\star$ denote the support of the sampling lattice associated to $\boldsymbol{G}$ in the dual space, $\boldsymbol{G}^\star = \operatorname{supp} \widehat{\text{Ш}}_{\boldsymbol{G}}$. For lattices, this is simply $\boldsymbol{L}^\star = \boldsymbol{L}^*$, but $\boldsymbol{D}$ is not a lattice, so it does not have a dual [3].

One can also write $\text{Ш}_{\boldsymbol{D}}$ as: $\text{Ш}_{\boldsymbol{D}} = (1 + s_{\boldsymbol{a}_2})\text{Ш}_{\boldsymbol{F}}(\boldsymbol{x})$. Using the shift property $\mathcal{F}(s_{\boldsymbol{v}} f) = e^{-\jmath 2\pi \boldsymbol{v}\cdot\boldsymbol{\xi}}\widehat{f}$ [17], one has $\widehat{\text{Ш}}_{\boldsymbol{D}} = (1 + e^{-\jmath 2\pi \boldsymbol{a}_2\cdot\boldsymbol{\xi}})\widehat{\text{Ш}}_{\boldsymbol{F}}$ [5]. It can then be shown that $e^{-\jmath 2\pi \boldsymbol{a}_2\cdot\boldsymbol{\xi}} = -1$ when $\boldsymbol{\xi} \in \boldsymbol{F}_4/\varepsilon^2$, so $\boldsymbol{D}^\star = \boldsymbol{P}_3/\varepsilon^2$.

The convolution theorem gives $\mathcal{F}(\text{Ш}_{\boldsymbol{G}} f) = (\widehat{\text{Ш}}_{\boldsymbol{G}} * \widehat{f})(\boldsymbol{\xi})$ [17], and since $(s_{\boldsymbol{v}}\delta * \widehat{f})(\boldsymbol{\xi}) = s_{\boldsymbol{v}}\widehat{f}(\boldsymbol{\xi})$, one has:[2]

$$\widehat{f}_{\boldsymbol{G}}(\boldsymbol{\xi}) = \sum_{\boldsymbol{v}\in\boldsymbol{G}^\star} s_{\boldsymbol{v}}\widehat{f}(\boldsymbol{\xi})\,, \quad \boldsymbol{\xi} \in \mathbb{R}^3\,. \tag{5}$$

The condition to avoid aliasing (spectral overlap) [1] is then $\bigcup_{\boldsymbol{v}\in\boldsymbol{G}^\star} \operatorname{supp} s_{\boldsymbol{v}}\widehat{f} = \{\}$. Let $\mathcal{M}_{\boldsymbol{G}}$ denote the largest $\operatorname{supp}\widehat{f}$ such that this condition is satisfied using $\text{Ш}_{\boldsymbol{G}}$. $\mathcal{M}_{\boldsymbol{L}}$ is also known as the *wavenumber cell* of the lattice $\boldsymbol{L}$ [1], [16]. In the dual space, a signal $\widehat{f}$ can be recovered from $\widehat{f}_{\boldsymbol{G}}$ with $\widehat{f} = \widehat{\mathcal{I}}_{\boldsymbol{G}}\widehat{f}_{\boldsymbol{G}}$, where $\widehat{\mathcal{I}}_{\boldsymbol{G}}$ is the indicator function $\widehat{\mathcal{I}}_{\boldsymbol{G}} = 1 : \boldsymbol{\xi} \in \mathcal{M}_{\boldsymbol{G}}, \widehat{\mathcal{I}}_{\boldsymbol{G}} = 0 : \boldsymbol{\xi} \notin \mathcal{M}_{\boldsymbol{G}}$. The signal recovery corresponds to $f(\boldsymbol{x}) = (\mathcal{I}_{\boldsymbol{G}} * f_{\boldsymbol{G}})(\boldsymbol{x})$, and as such, $\mathcal{I}_{\boldsymbol{G}}$ is also known as the *ideal interpolant* of the sampling lattice $\text{Ш}_{\boldsymbol{G}}$ [2].

Let $\mathcal{V}_{\boldsymbol{G}^\star,\boldsymbol{v}}$ denote the Voronoi cell at the origin in the shifted grid $\boldsymbol{G}^\star - \boldsymbol{v}$ for $\boldsymbol{v} \in \boldsymbol{G}^\star$ and let $\mathcal{N}_{\boldsymbol{G}^\star,\boldsymbol{v},n}$ denote the set of points in the nth shell of $\boldsymbol{G}^\star - \boldsymbol{v}$ (the nth *shell* is a set of points with equal distance from the origin, in increasing order of distance [3]). Any cell $\mathcal{V}_{\boldsymbol{G}^\star,\boldsymbol{v}}$ can then be written as the set of solutions to a system of linear inequalities: $\mathcal{V}_{\boldsymbol{G}^\star,\boldsymbol{v}} = \{\boldsymbol{\xi} \in \mathbb{R}^3 : 2\boldsymbol{\gamma}_{\boldsymbol{G}^\star,\boldsymbol{v},n}\cdot\boldsymbol{\xi} < \|\boldsymbol{\gamma}_{\boldsymbol{G}^\star,\boldsymbol{v},n}\|^2\}$, where $\boldsymbol{\gamma}_{\boldsymbol{G}^\star,\boldsymbol{v},n} \in \mathcal{N}_{\boldsymbol{G}^\star,\boldsymbol{v},n}$ and $n > 0$. In general, the intersection of these cells will be the largest support to avoid overlap (aliasing): $\mathcal{M}_{\boldsymbol{G}} = \bigcap_{\boldsymbol{v}\in\boldsymbol{G}^\star} \mathcal{V}_{\boldsymbol{G}^\star,\boldsymbol{v}}$. So the condition becomes $\mathcal{M}_{\boldsymbol{G}} = \{\boldsymbol{\xi} \in \mathbb{R}^3 : 2\boldsymbol{\gamma}_{\boldsymbol{G}^\star}\cdot\boldsymbol{\xi} < \|\boldsymbol{\gamma}_{\boldsymbol{G}^\star}\|^2\}$, where $\boldsymbol{\gamma}_{\boldsymbol{G}^\star} \in \bigcup_{\boldsymbol{v}\in\boldsymbol{G}^\star}\bigcup_{n>0}\mathcal{N}_{\boldsymbol{G}^\star,\boldsymbol{v},n}$. This can be simplified for lattices: $\mathcal{M}_{\boldsymbol{L}} = \mathcal{V}_{\boldsymbol{L}^*,\boldsymbol{0}}$ [1], as seen in Fig. 2(a) for $\mathcal{M}_{\boldsymbol{F}}$. There are three cells to consider on $\boldsymbol{D}^\star$, one for each $\boldsymbol{F}_i \subset \boldsymbol{P}_3$, as seen in Fig. 2(b). While $\boldsymbol{F}_4 \not\subset \boldsymbol{P}_3$, $\boldsymbol{F}_1 \cup \boldsymbol{F}_4 = \mathbb{Z}^3 \subset \boldsymbol{P}_4$ and $\boldsymbol{F}_2 \cup \boldsymbol{F}_3 = \mathbb{Z}^3 + \boldsymbol{a}_2 \subset \boldsymbol{P}_3$, so one has $\bigcup_{i=1}^3 \mathcal{N}_{\boldsymbol{D}^\star,\boldsymbol{v}_i,n} = \mathcal{N}_{\boldsymbol{F}^\star,\boldsymbol{0},n}$, where $\boldsymbol{v}_i \in \boldsymbol{F}_i/\varepsilon^2$. Thus, $\mathcal{M}_{\boldsymbol{D}} = \mathcal{M}_{\boldsymbol{F}}$, as demonstrated in Fig. 2(c). As such, the extra samples given by the points $\boldsymbol{F}_2 \subset \boldsymbol{D}$ are *redundant* and it follows that $\mathcal{I}_{\boldsymbol{D}} = \mathcal{I}_{\boldsymbol{F}}$.

While $\widehat{\text{Ш}}_{\boldsymbol{D}}$ was derived correctly in [5], the subsequent conclusions are mistaken. Fixing $\varepsilon = 1$, it was claimed that $\mathcal{M}_{\boldsymbol{D}}$ is a cube with vertices $\boldsymbol{\xi} = (1,0,0) + (\pm\frac{1}{2} \pm \frac{1}{2} \pm \frac{1}{2})$ [5]. However, according to Eq. (5), $\widehat{f}$ only replicates at $\boldsymbol{\xi} \in \boldsymbol{D}^\star$ and $(1,0,0) \notin \boldsymbol{D}^\star$ when $\varepsilon = 1$, so this cube is irrelevant.

[2]This assumes $\widehat{\text{Ш}}_{\boldsymbol{G}}$ is some sort of Dirac comb, which is the case for the grids considered here ($\boldsymbol{P}_M$), but is not always the case for irregular grids.

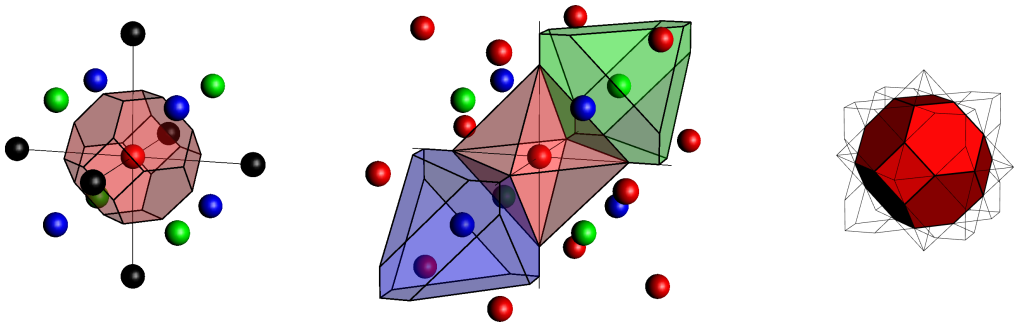

(a) (b) (c)

Fig. 2: (a) Voronoi cell of $\boldsymbol{P}_4$. (b) Voronoi cells of $\boldsymbol{P}_3$. (c) Intersection of three Voronoi cells from $\boldsymbol{P}_3$.

III. The Tetrahedral DWM

A. Finite difference scheme and digital waveguide mesh

Using the short-hand notation $\partial_w^2 = \frac{\partial^2}{\partial w^2}$ for some variable $w \in \mathbb{R}$, the 3-D wave equation can be written as:

$$\left(\partial_t^2 - c^2\Delta\right) u = 0\,, \quad \Delta = \partial_{x_1}^2 + \partial_{x_2}^2 + \partial_{x_3}^2\,, \tag{6}$$

where c is the wave speed, Δ is the 3-D Laplacian, t is time, and $u = u(\boldsymbol{x}, t)$ is a solution to be approximated for $t \in \mathbb{T}$, where $\mathbb{T} = \{t \in \mathbb{R} : t \geq 0\}$ and $\boldsymbol{x} \in \mathbb{R}^3$ (boundary conditions are not considered) given some initial conditions at $t = 0$.

Let $\tilde{u} = \tilde{u}(\boldsymbol{x}, t)$ represent the approximation to $u(\boldsymbol{x}, t)$. An approximation to ∂_t^2 is given by the FD operator $\delta_{tt,k}$:

$$\delta_{tt,k}\tilde{u} = \frac{1}{k^2}(\tilde{u}(\boldsymbol{x}, t+k) - 2\tilde{u}(\boldsymbol{x}, t) + \tilde{u}(\boldsymbol{x}, t-k))\,, \tag{7}$$

where k is the time-step, which can be chosen to be $k = 1/F_s$, where F_s is an audio rate (e.g. 44.1 kHz).

Let $\Omega \subset \mathbb{R}^3$ be a finite set of unit-norm vectors and let $|\Omega|$ denote its cardinality. For certain choices of Ω an approximation to the Laplacian can be written as:

$$\delta_{\Delta,\Omega,h}\tilde{u} = \frac{\kappa}{h^2}\sum_{i=1}^{|\Omega|}\left(\tilde{u}(\boldsymbol{x} + \boldsymbol{v}_i h, t) - \tilde{u}(\boldsymbol{x}, t)\right)\,, \tag{8}$$

where h is the spatial step, $\boldsymbol{v}_i \in \Omega$, and κ is chosen according to consistency conditions. On $\boldsymbol{D}$, an approximation to the Laplacian is given by two sets of four vectors: $\Omega_{D_1} = \frac{2}{\sqrt{3}\varepsilon}\mathcal{N}_{\boldsymbol{D},\boldsymbol{0},1}$ when $\boldsymbol{x} \in \boldsymbol{F}_1$ and $\Omega_{D_2} = -\Omega_{D_1}$ when $\boldsymbol{x} \in \boldsymbol{F}_2$, with $\kappa_D = 3/2$ for both orientations. On $\boldsymbol{F}$, an approximation is given by the set of twelve vectors: $\Omega_F = \frac{1}{\sqrt{2}\varepsilon}\mathcal{N}_{\boldsymbol{F},\boldsymbol{0},1}$ and $\kappa_F = 1/2$.

Typically, a FD approximation $\tilde{u}(\boldsymbol{x}, t)$ is only calculated at a set of points in space and time pertaining to the temporal grid $\boldsymbol{T} = \{nk : n \in \mathbb{N}\}$ ($0 \in \mathbb{N}$) and some spatial grid $\boldsymbol{G}$. The FD scheme for Eq. (6) is then:

$$(\delta_{tt,k} - c^2 \delta_{\Delta,\Omega,h})\tilde{u} = 0\,, \quad \boldsymbol{x} \in \boldsymbol{G}, t \in \boldsymbol{T}\,. \tag{9}$$

The FD approximation is *discretised*, but in this case, the discrete values are calculated with an explicit recursion in time:

$$\tilde{u}(\boldsymbol{x}, t+k) = (c^2 k^2 \delta_{\Delta,\Omega,h} + 2)\tilde{u}(\boldsymbol{x}, t) - \tilde{u}(\boldsymbol{x}, t-k)\,, \tag{10}$$

given some initial conditions. At each $t \in \boldsymbol{T}$, the discretised approximation $\tilde{u}(\boldsymbol{x}, t) : \boldsymbol{x} \in \boldsymbol{G}$ uniquely represents a continuous approximation $\tilde{u}(\boldsymbol{x}, t) : \boldsymbol{x} \in \mathbb{R}^3$ that can be reconstructed with $\mathcal{I}_{\boldsymbol{G}}$ as described in Section II. It follows that the maximum support of the continuous approximation will be $\mathcal{M}_{\boldsymbol{G}}$ in the wavenumber space ($\boldsymbol{\xi} \in \mathbb{R}^3$).

Let $h_{\boldsymbol{G}}$ be the distance between nearest neighbouring points in $\boldsymbol{G}$. The FD scheme in (9) becomes the 13-point FCC scheme with $\boldsymbol{G} = \boldsymbol{F}$ and $\delta_{\Delta,\Omega,h} = \delta_{\Delta,\Omega_F,h_{\boldsymbol{F}}}$. Similarly, for the tetrahedral FD scheme, $\boldsymbol{G} = \boldsymbol{D}$ and $\delta_{\Delta,\Omega,h} = \delta_{\Delta,\Omega_{D_i},h_{\boldsymbol{D}}}$ for $\boldsymbol{x} \in \boldsymbol{F}_i : i \in \{1, 2\}$. Note that $h_{\boldsymbol{F}} = \sqrt{8/3} h_{\boldsymbol{D}}$. The *tetrahedral DWM* [7] is a special case of the tetrahedral FD scheme [8]. When the Courant number $\lambda_{\boldsymbol{D}} = ck/h_{\boldsymbol{D}}$ is chosen to be $\lambda_{\boldsymbol{D}} = \sqrt{1/3}$, the tetrahedral FD scheme can be equivalently expressed in the wave-scattering formulation known as the DWM [8]. Similarly, when the 13-point FCC scheme has $\lambda_{\boldsymbol{F}} = ck/h_{\boldsymbol{F}} = \sqrt{1/3}$, it can be expressed as the "dodecahedral DWM" [4]. The equivalent DWM wave-scattering formulations are left out for brevity, but details can be found in [4], [7], [8], [12].

B. Decoupling in space and time

As space and time are linked in the FD scheme, the temporal and spatial grids can be viewed as one combined *spatiotemporal* grid. For example, the spatiotemporal grid for the tetrahedral scheme is $\boldsymbol{D} \times \boldsymbol{T}$, where $\times$ denotes the Cartesian product. Consider the two staggered temporal grids: $\boldsymbol{T}'_j = \left\{\left(n + \frac{(j-1)}{2}\right) k' : n \in \mathbb{N}, j \in \{1, 2\}\right\}$ where $k' = 2k$. Four spatiotemporal subgrids can be defined by taking the Cartesian products: $\boldsymbol{F}_i \times \boldsymbol{T}'_j$ for $(i, j) \in \{1, 2\} \times \{1, 2\}$. The union of these four spatiotemporal subgrids is $\boldsymbol{D} \times \boldsymbol{T}$.

To establish consistency with the wave equation and to subsequently analyse numerical dispersion, the tetrahedral DWM, when first presented, was rewritten over *two time-steps* as the following FD scheme [7]:

$$\sum_{j=0}^{2} \tilde{u}(\boldsymbol{x}, t - 2jk) - \frac{1}{4} \sum_{i=1}^{12} \tilde{u}(\boldsymbol{x} + \boldsymbol{v}_i h_{\boldsymbol{F}}, t - 2k) = 0\,, \tag{11}$$

where $\boldsymbol{v}_i \in \Omega_F$ ($\mathcal{N}_{\boldsymbol{D},\mathbf{0},2} = \mathcal{N}_{\boldsymbol{F},\mathbf{0},1}$) and $(\boldsymbol{x}, t) \in \boldsymbol{D} \times \boldsymbol{T}$. After accounting for a time-shift by k', (11) is simply:

$$\tilde{u}(\boldsymbol{x}, t + k') = (c^2 k'^2 \delta_{\Delta,\Omega_F,h_{\boldsymbol{F}}} + 2)\tilde{u}(\boldsymbol{x}, t) - \tilde{u}(\boldsymbol{x}, t - k')\,, \tag{12}$$

where $(\boldsymbol{x}, t) \in \boldsymbol{D} \times \boldsymbol{T}$ and with a Courant number $\lambda'_{\boldsymbol{F}} = ck'/h_{\boldsymbol{F}} = \sqrt{1/2}$, which is the stability limit of this FD scheme [8], [16]. Eq. (12) can then be written as the following set of 13-point FD schemes locally operating on four spatiotemporal subgrids:

$$(\delta_{tt,k'} - c^2 \delta_{\Delta,\Omega_F,h_{\boldsymbol{F}}})\tilde{u} = 0\,, \quad (\boldsymbol{x}, t) \in \boldsymbol{F}_i \times \boldsymbol{T}'_j \tag{13}$$

for $(i, j) \in \{1, 2\} \times \{1, 2\}$. Since the subgrids are disjoint in space and time, this describes *four decoupled subschemes* that can be used independently to arrive at exactly the same result as the combined tetrahedral DWM scheme, as long as the initial conditions for (13) agree with those of the tetrahedral DWM. Furthermore, the values: $\tilde{u}(\boldsymbol{x}, t) : (\boldsymbol{x}, t) \in \boldsymbol{F}_1 \times \boldsymbol{T}'_1$ are sufficient to uniquely represent $\tilde{u}(\boldsymbol{x}, t) : \boldsymbol{x} \in \mathbb{R}^3, t \in \mathbb{T}$ since $\mathcal{M}_{\boldsymbol{D}} = \mathcal{M}_{\boldsymbol{F}}$ and because $\tilde{u}(\boldsymbol{x}, t)$ only depends on $\tilde{u}(\boldsymbol{x}, t - k')$ and $\tilde{u}(\boldsymbol{x}, t - 2k')$. These values can be calculated with only one FCC subscheme in (13). In other words, the tetrahedral DWM is essentially a redundant formulation of a 13-point FD scheme on the FCC grid.

The tetrahedral FD scheme can also be written as two interleaved subschemes:

$$(\delta_{tt,k} - c^2 \delta_{\Delta,\Omega_{D_i},h_{\boldsymbol{D}}})\tilde{u} = 0\,, \quad (\boldsymbol{x}, t) \in \boldsymbol{F}_i \times \boldsymbol{T}'_j\,. \tag{14}$$

where $(i, j) \in \{1, 2\} \times \{1, 2\}$, and where each subscheme requires a pair of spatiotemporal subgrids: $i = j$ or $i \neq j$. Employing only one subscheme is known as the "chessboard technique" [4], [8], and this is also sufficient to represent $\tilde{u}(\boldsymbol{x}, t) : \boldsymbol{x} \in \mathbb{R}^3, t \in \mathbb{T}$.

C. Simulation

To verify the equivalence between the tetrahedral DWM and the FCC subschemes, a simulation was run on a 1 m^3 domain with $k = 1/F_s$, $F_s = 44.1$ kHz, $c = 343$ m/s, and using double floating-point precision. An energy-normalised 3-D spatial Gaussian function (centered in space, fixed in time) was used as an initial condition, with a variance of 0.05. One simulation was computed using the tetrahedral DWM and another using the decoupled FCC subschemes in (13), although in the latter case, the first time-step was computed using the tetrahedral DWM so that initial conditions matched. Some values of $\tilde{u}(\boldsymbol{x}, t)$ over time at a point along an axis and 0.2 m from the center are shown in Fig. 3(a). The difference between the two simulations is negligible, as seen in Fig. 3(b). Furthermore, decoupling in time can be seen in Fig. 3(a) as an apparent low-amplitude, high-frequency oscillation; this is in fact two smooth wave fronts interleaved in time.

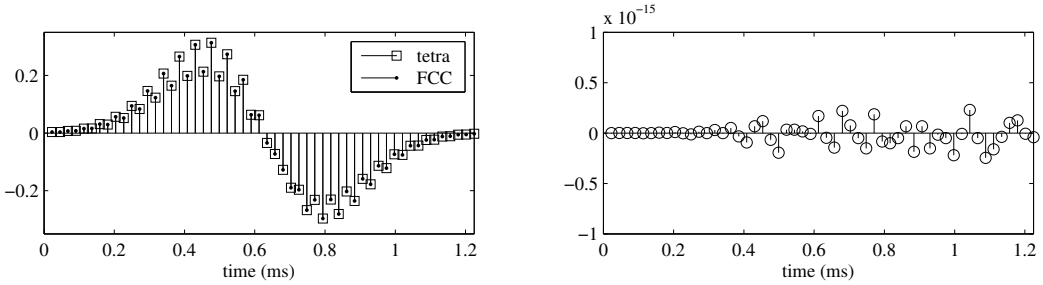

(a) (b)

Fig. 3: (a) Output of simulation with Gaussian initial condition. (b) Difference between the two calculations in (a).

D. Numerical Dispersion and Computational Efficiency

In practice, boundary conditions are imposed and a forcing term is usually added to Eq. (6) to represent a point source for room acoustics applications. As these features were not considered, inconsistencies can arise between the tetrahedral DWM and the FCC subschemes in practice. However, one critical issue for 3-D room acoustics applications is the wave speed error due to numerical dispersion, and this does not take into consideration any such features. Numerical dispersion can be analysed by considering a plane wave of the form: $\tilde{u}(\boldsymbol{x}, t) = e^{j(\omega t + \boldsymbol{\xi}\cdot\boldsymbol{x})}$, where $\omega \in \mathbb{R}$ is the temporal frequency. Inserting the plane wave into (11), and after simplifying, one obtains:

$$z^{-4} + b(\boldsymbol{\xi}) z^{-2} + 1 = 0\,, \quad b(\boldsymbol{\xi}) = 1 - \frac{1}{4}\sum_{i=1}^{12} e^{\jmath \boldsymbol{\xi}\cdot\boldsymbol{v}_i h_{\boldsymbol{F}}}\,, \tag{15}$$

where $\boldsymbol{v}_i \in \Omega_F$ and $z = e^{\jmath\omega k}$. This expression is equivalent to what is found by taking the Z-transform and spatial FT of the scheme [7]. The solution to this quadratic expression in z^{-2}, $G(\boldsymbol{\xi}) = \frac{1}{2}(-b \pm \sqrt{b^2 - 4})$, is the *spectral amplification factor* [7], [8] of the tetrahedral scheme over *two time-steps*. In other words, one can advance the scheme using the following *pseudospectral* update: $\mathcal{F}(\tilde{u})(\boldsymbol{\xi}, t + 2nk) = G^n(\boldsymbol{\xi})\mathcal{F}(\tilde{u})(\boldsymbol{\xi}, t)$, where $\mathcal{F}(\tilde{u})(\boldsymbol{\xi}, t)$ is the spatial FT of $\tilde{u}(\boldsymbol{x}, t)$. Note that b is real due to the symmetry in Ω_F and $|b| \leq 2$. Furthermore, $|G(\boldsymbol{\xi})| = 1$ (no dissipation). There are two *one-step* amplification factors from $\sqrt{G(\boldsymbol{\xi})}$, one of which can produce undesirable *parasitic modes* [8]. Considering (11)-(13), it follows that $G(\boldsymbol{\xi})$ is also the *one-step* spectral amplification factor of the FCC scheme with the time-step k' when $\lambda'_{\boldsymbol{F}} = \sqrt{1/2}$.

Numerical dispersion gives rise to a numerical phase velocity that deviates from the ideal wave speed c with a directional dependence. The numerical phase velocity of the tetrahedral scheme can be written

as [8]: $\nu_D(\boldsymbol{\xi}) = |(\jmath k\|\boldsymbol{\xi}\|)^{-1} \log G^{\frac{1}{2}}|$ for $\boldsymbol{\xi} \in \mathcal{M}_{\boldsymbol{D}}$. For the FCC scheme, the numerical phase velocity is: $\nu_F(\boldsymbol{\xi}) = |(\jmath k'\|\boldsymbol{\xi}\|)^{-1} \log G|$ for $\boldsymbol{\xi} \in \mathcal{M}_{\boldsymbol{F}}$. Clearly, $\nu_D(\boldsymbol{\xi}) = \nu_F(\boldsymbol{\xi})$ and since $\mathcal{M}_{\boldsymbol{F}} = \mathcal{M}_{\boldsymbol{D}}$, the two schemes have the same numerical phase velocity for the entire range of spatial frequencies that can be discretised on the grids. Some further analysis of $\nu_D(\boldsymbol{\xi})$ can be found in [7], although $\mathcal{M}_{\boldsymbol{D}}$ was assumed to be a cube. See [16] for $\nu_F(\boldsymbol{\xi})$ with $\boldsymbol{\xi} \in \mathcal{M}_{\boldsymbol{F}}$ (a truncated octahedron).

One FCC subscheme in (13) uses one spatiotemporal subgrid, so its *computational density*, which is the density of the spatiotemporal grid [8], [13], [16], is one-quarter that of the tetrahedral FD scheme. Since only one spatial subgrid is used, memory storage is also halved. The chessboard technique uses twice the memory and computational density of one FCC subscheme since it requires an interleaved pair of spatiotemporal subgrids. For large-scale 3-D simulations on GPUs, memory storage and memory bandwidth (density of memory reads) are limiting factors [15], [18]. The tetrahedral scheme requires five memory reads per update while the FCC scheme requires 14, so the memory bandwidth is 30% lower for the FCC scheme. The chessboard technique also requires five memory reads, so its memory bandwidth is 23% lower than one FCC subscheme, although the doubled memory storage outweighs this advantage. It is well-known that 3-D DWMs use more computational resources than their equivalent FD counterparts [9], [19] so savings can be greater when compared to the actual tetrahedral DWM implementation.

The *computational efficiency* of FD schemes can be compared in terms of the computational densities required to keep the wave speed error ($|c-\nu(\boldsymbol{\xi})|$) below some threshold, up to some critical frequency [13], [16]. It is straightforward to compare the tetrahedral and FCC schemes in this regard since $\nu_D(\boldsymbol{\xi}) = \nu_F(\boldsymbol{\xi})$ for the entire range of discretised spatial frequencies; the computational efficiency of the FCC scheme is four times that of the tetrahedral scheme for any measure of wave speed error.

IV. Conclusion

It has been shown that the spatial frequency support (bandwidth) of a signal discretised on the diamond grid is limited to the wavenumber cell of a sparser FCC grid. As a consequence, half of the samples from a diamond sampling lattice are redundant when sampling a bandlimited signal. The tetrahedral DWM was shown to decouple into four 13-point FD schemes on FCC subgrids and this was verified with a simulation. Numerical dispersion was discussed to show that the 13-point FD scheme on the FCC grid is four times more efficient than the tetrahedral DWM in terms of minimising wave speed error. With these results, it can be concluded that the 13-point FD scheme on the FCC grid is a better choice than the tetrahedral DWM for large-scale room acoustics simulations.

REFERENCES

[1] D. P. Petersen and D. Middleton, "Sampling and reconstruction of wave-number-limited functions in N-dimensional Euclidean spaces," *Information and control*, vol. 5, no. 4, pp. 279–323, 1962.

[2] W. Ye and A. Entezari, "A geometric construction of multivariate sinc functions," *IEEE Trans. Image Processing*, vol. 21, no. 6, pp. 2969–2979, 2012.

[3] J. Conway and N. J. A. Sloane, *Sphere packings, lattices and groups*. Springer-Verlag, 1988.

[4] G. R. Campos and D. M. Howard, "On the computational efficiency of different waveguide mesh topologies for room acoustic simulation," *IEEE Trans. Speech and Audio Processing*, vol. 13, no. 5, pp. 1063–1072, 2005.

[5] R. Strand, "Sampling and ideal reconstruction on the 3D diamond grid," in *IEEE Int. Conf. Pattern Recognition (ICPR)*, 2010, pp. 4609–4612.

[6] G. E. Forsythe and W. R. Wasow, *Finite-difference methods for partial differential equations*. New York: Wiley, 1960.

[7] S. A. van Duyne and J. O. Smith III, "The tetrahedral digital waveguide mesh," in *Proc. IEEE WASPAA*, New Paltz, NY, 1995, pp. 234–237.

[8] S. Bilbao, "Wave and scattering methods for the numerical integration of partial differential equations," Ph.D. thesis, Stanford University, 2001.

[9] V. Välimäki, J. D. Parker, L. Savioja, J. O. Smith III, and J. S. Abel, "Fifty years of artificial reverberation," *IEEE Trans. Audio, Speech, and Language Processing*, vol. 20, no. 5, pp. 1421–1448, 2012.

[10] L. Savioja, T. J. Rinne, and T. Takala, "Simulation of room acoustics with a 3-D finite difference mesh," in *Proc. Int. Computer Music Conf. (ICMC)*, Danish Institute of Electroacoustic Music, 1994, pp. 463–466.

[11] G. Campos and D. Howard, "A parallel 3D digital waveguide mesh model with tetrahedral topology for room acoustic simulation," in *Proc. Digital Audio Effects (DAFx)*, Verona, Italy, 2000, pp. 73–78.

[12] S. Miklavcic and J. Ericsson, "Practical implementation of the 3D tetrahedral TLM method and visualization of room acoustics," in *Proc. Digital Audio Effects (DAFx)*, Naples, Italy, 2004, pp. 262–267.

[13] K. Kowalczyk and M. van Walstijn, "Room acoustics simulation using 3-D compact explicit FDTD schemes," *IEEE Trans. Audio, Speech, and Language Processing*, vol. 19, no. 1, pp. 34–46, 2011.

[14] F. Fontana and D. Rocchesso, "Signal-theoretic characterization of waveguide mesh geometries for models of two-dimensional wave propagation in elastic media," *IEEE Trans. Speech and Audio Processing*, vol. 9, no. 2, pp. 152–161, 2001.

[15] C. J. Webb and A. Gray, "Large-scale virtual acoustics simulation at audio rates using three dimensional finite difference time domain and multiple GPUs," in *Proc. Int. Cong. Acoustics (ICA)*, Montréal, 2013.

[16] B. Hamilton and S. Bilbao, "On finite difference schemes for the 3-D wave equation using non-Cartesian grids," in *Proc. Sound and Music Computing (SMC) Conf.*, Stockholm, Sweden, 2013, pp. 592–599.

[17] D. Dudgeon and R. Mersereau, "Multidimensional digital signal processing," *Englewood Cliffs: Prentice-Hall*, vol. 1, 1984.

[18] B. Hamilton and C. J. Webb, "Room acoustics modelling using GPU-accelerated finite difference and finite volume methods on a face-centered cubic grid," in *Proc. Digital Audio Effects (DAFx)*, Maynooth, Ireland, Sep. 2013.

[19] L. Savioja, T. J. Rinne, and T. Takala, "Simulation of room acoustics with a 3-D finite difference mesh," in *Proc. Int. Computer Music Conf. (ICMC)*, Danish Institute of Electroacoustic Music, Denmark, 1994, pp. 463–466.